Vieira de Castro Martins Antao, Tiago; Lado, Jose; Otero Fumega, Adolfo

Electric Field Control Of Moiré Skyrmion Phases in Twisted Multiferroic NiI2 Bilayers

Published in:
Nano Letters

DOI:
10.1021/acs.nanolett.4c04582

Published: 11/12/2024

Document Version
Publisher's PDF, also known as Version of record

NANO LETTERS

pubs.acs.org/NanoLett
Letter

Electric Field Control Of Moiré Skyrmion Phases in Twisted Multiferroic NiI_2 Bilayers

Tiago V. C. Antão,* Jose L. Lado,* and Adolfo O. Fumega*

Cite This: *Nano Lett.* 2024, 24, 15767−15773
Read Online

ACCESS | Metrics & More | Article Recommendations | Supporting Information

ABSTRACT: Twisted magnetic van der Waals materials provide a flexible platform to engineer unconventional magnetism. Here we demonstrate the emergence of electrically tunable topological moiré magnetism in twisted bilayers of the spin-spiral multiferroic NiI_2. We establish a rich phase diagram featuring uniform spiral phases, a variety of $k\pi$-skyrmion lattices, and nematic spin textures ordered at the moiré scale. The emergence of these phases is driven by the local stacking and the resulting moiré modulated frustration. Notably, when the spin-spiral wavelength is commensurate with the moiré length scale by an integer k, multiwalled skyrmions become pinned to the moiré pattern. We show that the strong magnetoelectric coupling displayed by the moiré multiferroic allows electric control of the $k\pi$-skyrmion lattices by an out-of-plane electric field. Our results establish a highly tunable platform for skyrmionics based on twisted van der Waals multiferroics, potentially enabling a new generation of ultrathin topologically protected spintronic devices.

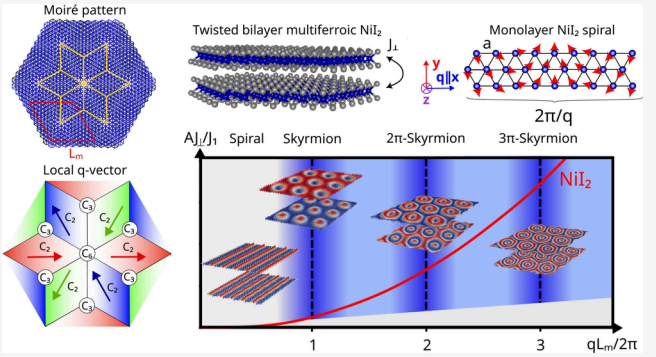

KEYWORDS: *2d multiferroics, skyrmions, van der Waals heterostructures, Twisted bilayer, moiré, frustrated magnetism*

Skyrmions are topologically protected magnetic structures that have garnered significant attention due to their potential applications in spintronics, particularly in the areas of data storage and manipulation.[1−4] These nanoscale spin textures are of great interest for advanced energy-efficient memory technologies because of their stability and unique spin configurations. Skyrmions have been observed or proposed in a variety of systems, including two-dimensional (2D) magnets,[5−8] magnetic thin films,[9] and material interfaces.[10] Their formation is typically driven by mechanisms such as the Dzyaloshinskii-Moriya (DM) interaction,[11,12] magnetic frustration,[13−17] and other types of magnetic anisotropy modulation.[18] Despite the excitement surrounding skyrmions, their emergence in insulating materials is relatively rare.[19−21] This presents a challenge for integrating skyrmions into insulating platforms, which are particularly attractive for low-power spintronic applications.

Two-dimensional van der Waals (vdW) materials provide an exciting new avenue for engineering exotic quantum phases of matter,[22] including the design of exotic magnetic phases.[23−25] The weak vdW bonding between the layers in this class of materials allows easily reach their monolayer limit, establishing a rich family of 2D building blocks.[26−34] The monolayers can be stacked together to generate heterostructures with emergent collective states.[35−37] Moreover, a twist angle can be introduced between stacked layers, giving rise to a moiré length scale that drives the emergence of complex phase diagrams.[38,39] For example, twisting has been shown to induce multiferroicity and skyrmionic patterns in bilayer chromium trihalides (CrX_3, X = Br, I, Cl)[40−47] and transition metal dichalcogenides.[48,49] Additionally, exotic magnetic orders, including whirls and stripes, have been proposed in twisted 2D magnets like $RuCl_3$.[50] The isolation of monolayer NiI_2,[51,52] has recently provided a new avenue for engineering matter by introducing multiferroic behavior as a new building block within magnetic vdW materials.[53−55] Multiferroic materials exhibit simultaneous electric and magnetic order.[56,57] In particular, NiI_2 is a type-II multiferroic whose ferroelectricity originates from its helical magnetic order and strong spin−orbit coupling[58] resulting in a strong magnetoelectric coupling.[52,59] It has been reported that the multiferroic order in NiI_2 can be tuned by external factors such as strain,[60] pressure,[61,62] substrate engineering[63] or cobalt substitution.[64] However, the emergence of exotic magnetic orders displaying strong magnetoelectric coupling in NiI_2 moiré heterostructures has remained unexplored.

In this paper, we demonstrate that twisted bilayer NiI_2 allows engineering topological magnetic textures, realizing a whole new family of multiferroic orders. We show that the moiré created by the twist angle enhances the frustration in the system and

Received: September 17, 2024
Revised: November 11, 2024
Accepted: November 14, 2024
Published: November 22, 2024

produces a variety of exotic magnetic orders, specifically exotic $k\pi$-skyrmions driven by the commensurability of the spin spiral wavelength and moiré length scale. Additionally, we show that the multiferroic order of twisted NiI_2 provides an unprecedented level of control over skyrmion lattice states using external electric fields, allowing driving the system between different skyrmionic configurations. We provide a phase diagram for the skyrmion phases in the twisted bilayer and demonstrate the electric-field tunability of these magnetic states, establishing twisted bilayer NiI_2 as a versatile platform for engineering and manipulating topological spin textures.

In monolayer NiI_2, multiferroicity emerges from the coexistence of a noncollinear magnetic spin-spiral order and strong spin−orbit coupling[58,65] via the inverse Dzyaloshinskii-Moriya (DM) effect.[66−68] This effect causes a noncentrosymmetric displacement of electric charge due to the noncollinear spin structure leading to an electric polarization. The magnetic ground state of monolayer NiI_2 corresponds to a coplanar spin spiral magnetic order (Figure 1(a)). The spin spiral phase arises

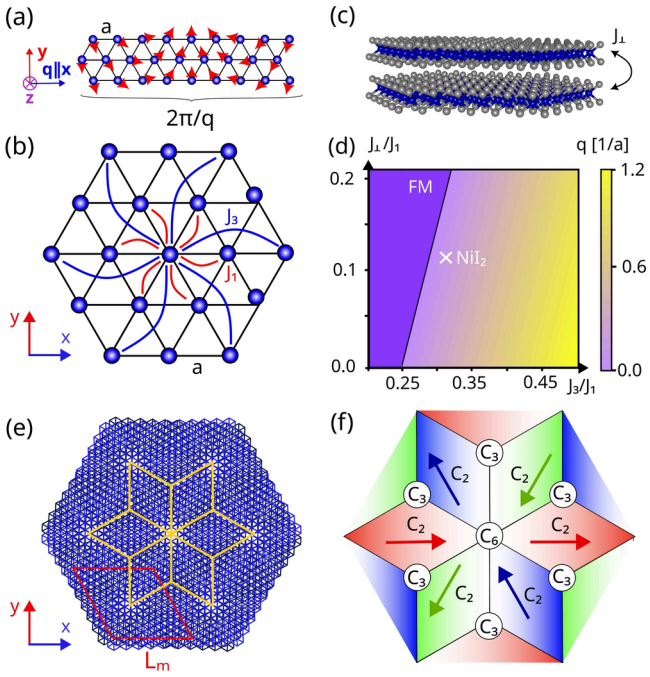

Figure 1. (a) Schematic of the spin-spiral of monolayer NiI_2 with wavelength $2\pi/q$.(b) Exchange interactions J_1 and J_3 of the Ni triangular lattice leading to the noncollinear spin-spiral state. (c) Schematic of a NiI_2 twisted bilayer, with Ni atoms represented in blue, and I atoms in gray. (d) Magnitude of the propagation vector q as a function of the interlayer exchanges $J_\perp/J_1$ and J_3/J_1. (e) Moiré pattern of twisted bilayer NiI_2, showing the moiré unit cell (red), and the spatial patches with C_2 symmetric rhombohedral stacking along different directions (yellow). (f) Schematic of the domains of q originated by the local broken symmetry.

from the magnetic frustration induced by the competition between ferromagnetic first-neighbor J_1 and antiferromagnetic third-neighbors J_3 magnetic exchange interactions[52,69,70] (Figure 1(b)). In the bulk limit, additional interactions, such as the Kitaev anisotropic interaction and biquadratic exchange, have also been proposed to influence the ground state spin configuration in NiI_2.[71] However, in the ultrathin limit, theoretical analyses have found these terms to be negligible,[63] and atomic-scale experiments have shown that a minimal classical Heisenberg $J_1 - J_3$ model suffices to accurately describe the observed ground state.[52] The magnetization in the spin-spiral phase of monolayer NiI_2 is described by propagation vector $\boldsymbol{q}$, determining the direction and wavelength $2\pi/q$ of the spin-spiral. The $\boldsymbol{q}$ vector is intrinsically constrained by the exchange interactions of the spin Hamiltonian to the direction of the first (or third) neighbors and its periodicity is determined by the J_3/J_1 ratio.[72,73] In particular, $J_3 \approx -0.3J_1$ is found to reproduce the experimentally observed spiral periodicity.[52] In addition, experimentally, the magnetization is observed to be mostly in-plane,[52] which is accounted for by an in-plane anisotropy term $A_z = -0.02J_1$, which fixes the rotation plane as $\hat{\boldsymbol{e}} = \hat{\boldsymbol{z}}$, as depicted in Figure 1(a). Other additional terms such as anisotropic symmetric exchange interactions may also play a role in fixing the direction of $\hat{\boldsymbol{e}}$ as well as changing the length-scale determined by the J_3/J_1 ratio,[20] however these should not contribute significantly to the results presented in the following discussion (see the S.I. for a detailed discussion). When two NiI_2 layers are stacked, an antiferromagnetic interlayer exchange $J_{\perp,(ij)}$ is established (Figure 1(c)). $J_{\perp,(ij)}$ is parametrized by an exponentially decaying function peaking at the next nearest interlayer neighbor distance at zero twist angle with strength $J_\perp$. The total Hamiltonian for twisted NiI_2 bilayer reads

$$H = J_1 \sum_{\langle i,j\rangle_1} \boldsymbol{S}_i \cdot \boldsymbol{S}_j + J_3 \sum_{\langle i,j\rangle_3} \boldsymbol{S}_i \cdot \boldsymbol{S}_j + A_z \sum_i (S_i^z)^2 + \sum_{\langle i,j\rangle_\perp} J_{\perp,(ij)} \boldsymbol{S}_i \cdot \boldsymbol{S}_j, \quad (1)$$

where $\langle \cdot,\cdot \rangle_n$ denotes the nth nearest neighbors and $\langle \cdot,\cdot \rangle_\perp$ refers to summation over sites in distinct layers. The emergence of distinct orders in the twisted bilayer arises from the additional frustration introduced by interlayer coupling (Figure 1(c)). Note that, as opposed to other twisted magnets,[40,41,50] the sign of $J_\perp$ does not have a stacking dependence, and the emerging orders in this system will be driven by the interplay between the spin-spiral and moiré length scales. A detailed *ab initio* analysis of the stacking dependence of $J_\perp$ in twisted NiI_2 is provided in the S.I. Physically, the presence of antiferromagnetic interlayer interactions causes a local antialignment of spins on the top and bottom layers resulting in the two layers having the same direction and magnitude of $\boldsymbol{q}$. The first effect of Figure 1(d) transitions from a ferromagnetic phase to a spin-spiral phase at a ratio of $J_3/J_1 = 0.25$ when $J_\perp = 0$, and this critical value is enhanced for $J_\perp > 0$. The value of the ratio J_3/J_1 for twisted bilayer NiI_2 is taken to be approximately the same as the monolayer, and the interlayer exchange is estimated to be given by $J_\perp/J_1 \approx -0.14$,[59,71] marked in the phase diagram Figure 1(d).

When the two layers are twisted, the phase diagram of Figure 1(d) is found to be unchanged up to twist angles of 6°, so the renormalization of the magnitude of $\boldsymbol{q}$ does not depend on the angle for small twist angles. However, the moiré pattern induces regions of higher spin density along certain spatial directions within each moiré unit cell, as illustrated in Figure 1(e). In Figure 1(f), the different colored regions correspond to areas of the moiré pattern where the rotational symmetry of the crystalline environment is broken from the monolayer C_6 down to a C_2 rhombohedral stacking, promoting the emergence of patches with well-defined q-vector directions. In the center of the moiré supercell, a C_6 symmetric monoclinic stacking area remains, where six q-vector patches coalesce. Additional C_3 symmetric regions appear, surrounded by three q-vector patches. This local modulation of $\boldsymbol{q}$ into a function of position

https://doi.org/10.1021/acs.nanolett.4c04582
Nano Lett. 2024, 24, 15767−15773

q_i is, contingent on the moiré supercell being large enough for these symmetries to approximately hold, as well as $J_\perp$ being strong enough relative to the moiré unit cell size L_m to generate a sufficiently strong pinning potential. Therefore, a finite twist angle between layers will introduce an extra moiré length scale L_m that will interplay with the spin spiral length scale q of each layer, thus giving rise to exotic magnetic scales.

We move on to computing the magnetic ground states arising from the model for twisted NiI_2 as a function of the competing spin spiral and moiré length scales. We find the lowest energy configurations under generalized twisted boundary conditions, which allows us to account for ground states where the spiral wavelength and moiré length scale are not commensurate. Two paradigmatic examples of the kind of topological magnetic phases achievable in twisted bilayer NiI_2 are the skyrmion and skyrmionium (2π-skyrmion) lattices[6,74−76] (see the S.I. for details on the calculation of the spin ground states). These are plotted in Figure 2(a) considering the commensurate cases $qL_m/2\pi = 1$ and $qL_m/2\pi = 2$, with twist angles $\theta \approx 3.89°$ and $\theta \approx 2.13°$ respectively. Only the top layer is showcased, although both layers are used in the calculation. The bottom layer is antiferromagnetically aligned with the top. Associated with these magnetic textures, in Figure 2(b) we computed the local q. The results match well with the schematic presented in Figure 1(f), confirming that the moiré length scale induces the pinning of the q vector directions. Finally, the presence of strong spin−orbit coupling λ induces an emergent electric polarization $P_{ij}=\lambda r_{ij} \times (S_i \times S_j)$ in noncollinear magnets.[66,67] Figure 2(c) shows the emergent polarization associated with the skyrmion and skyrmionium lattices in the top layer of the twisted NiI_2 system. The bottom layer has an identical polarization profile. It can be seen that the emergent polarization points mostly in the out-of-plane direction z. This starkly contrasts with the monolayer case and is a key feature that allows the twisted bilayer to couple to out-of-plane electric fields. In the twisted bilayer system, the microscopic mechanism that originates ferroelectric polarization is the same as in the monolayer, namely the inverse DM mechanism.[67] However, it is the emergent noncoplanar magnetic order driven by the moiré scale frustration that results in a dominantly out-of-plane component. This is the key difference distinguishing the magnetic and ferroelectric orders in the twisted bilayer from those found in the monolayer. The novel multiferroic behavior found in the bilayer also allows for the magnetic control of ferroelectricity. This feature allows us to distinguish it from the sliding ferroelectricity emerging in other twisted systems (such as twisted boron nitride bilayers),[77] for which the driving mechanism is the lattice distortions stemming from relaxation effects. For twisted bilayer NiI_2, we expect that atomic relaxations will not produce large effects on the magnetic order and the expected phase diagram for the system (see the Supporting Information for details on the effect of atomic lattice relaxations on the magnetic order).

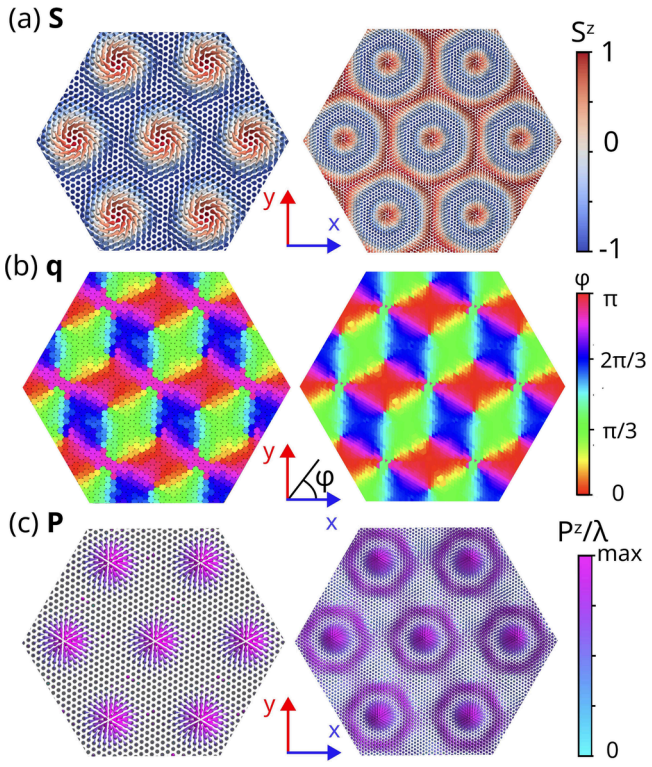

Figure 2. (a) Spin S, (b) propagation vector q, and (c) polarization P of a skyrmion and skyrmionium lattice in twisted bilayer NiI_2. These occur for twist angles $\theta \approx 3.89°$ and $\theta \approx 2.13°$, left and right panels, respectively. The panels show the top layer of a twisted bilayer, with the bottom one featuring a magnetic configuration that is antialigned with the top, and an equivalent polarization profile.

The ground-state solutions as a function of the twist angle are presented in the phase diagram shown in Figure 3(a). Variations in the twist angle and $J_\perp$ allow for the identification of many other topologically distinct phases. This phase diagram shows many topologically distinct phases as a function of the commensurability parameter qL_m and the interlayer coupling $J_\perp$. The transition into the spiral phase is found to be approximately linear when $J_\perp$ is normalized by the moiré area $\sim L_m^2$, which leads to a choice of vertical axis for the phase diagram of the form $J_\perp L_m^2/J_1 a^2$. The spin spiral phase occurs when $J_\perp/J_1$ is small or the twist angle is large, making L_m too small to impact the interlayer exchange field significantly (Figure 3(b)). However, the direction of q is changed from the third neighbors to the moiré superlattice vectors. A series of other phases corresponding to $k\pi$-skyrmion or so-called target skyrmion lattices emerge at integer values of $qL_m/2\pi = k$ ($k \in \mathbb{N}$), when the moiré unit cell accommodates an integer number of spin-spiral wavelengths (Figures 3(c,e,g)). Another family of phases corresponds to nematic skyrmion lattices (Figures 3(d,f)), which occur for twist angles that lead to incommensurate values of q and L_m. This produces whirling textures within each unit cell and breaks translational symmetry differently for each moiré lattice vector compared to the commensurate case. Therefore, these nematic phases can host coexisting skyrmion and spiral features.

It is worth noting that the distinct emergent phases can be distinguished based on topological features. In particular, the topology of the configuration depends on the distribution of the ferromagnetic chains and how they accommodate the local q-vector. These chains can form concentric loops corresponding to skyrmionic textures, or cross the borders of the moiré unit cell, leading to helical and nematic textures. For noninteger qL_m values, for instance, chains are deformed in such a way as to form horseshoe patterns, or other distinct whirls, locally breaking the described q patches into smaller regions, but preserving some of the global topological features of the spin configuration, such as the total winding $k\pi$. In general, the textures found in between $k\pi$ and $(k+1)\pi$ Skyrmion lattices can have any winding $p \in \mathbb{N}$ with $0 \le p < k+1$. The presence of these topological features points to potential stability under external perturbations.

https://doi.org/10.1021/acs.nanolett.4c04582
Nano Lett. 2024, 24, 15767−15773

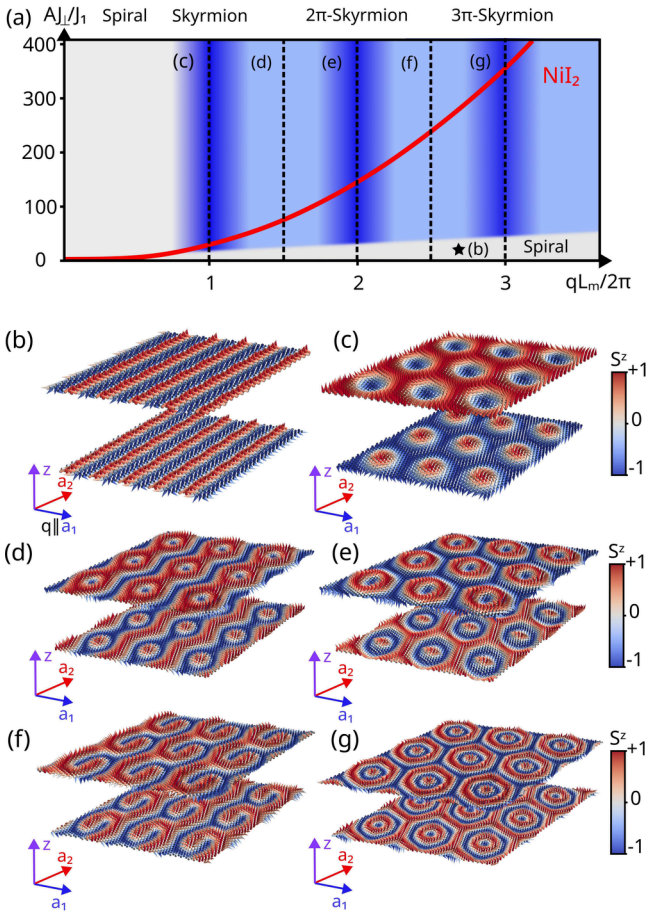

Figure 3. (a) Phase diagram of twisted bilayer NiI_2 as a function of normalized interlayer exchange $AJ_\perp/J_1$ and $qL_m/2\pi$. The factor $A = L_m^2/a^2$ introduces the relative area between the moiré and the single unit cells, ensuring that the same ground states are represented along vertical lines in the phase diagram. The red line represents NiI_2 as L_m increases or, equivalently, as the twist angle becomes smaller. (b-g) Representative ground state solutions of the moiré spin-spiral multiferroic bilayer phase diagram shown in panel (a): (b) uniform spin spiral; (c), (e), and (g) the simple, 2π- and 3π-skyrmion lattices, respectively; and (d) and (f) intermediate phases with nematic order between commensurate solutions.

Electric field control: We now address the effect of an external out-of-plane electric field on the ground-state spin configuration in these $k\pi$-skyrmion lattice phases. The strong magnetoelectric coupling in multiferroics is particularly attractive to control skyrmion lattices. An external uniform electric field $\boldsymbol{E}_{ext}$ couples to the associated electric polarization $\boldsymbol{P}_{ij}$ generated via the inverse DM. This introduces a magnetoelectric coupling term in the Hamiltonian of the form $H_{ME} = -\sum_{\langle ij\rangle}\boldsymbol{E}_{ext}\cdot\boldsymbol{P}_{ij}$. The microscopic formula of the electric polarization leads to a term of the form

$$H_{ME} = -\lambda E_\perp \sum_{\langle ij\rangle} (\hat{z}\times \boldsymbol{r}_{ij})\cdot(\boldsymbol{S}_i \times \boldsymbol{S}_j) \tag{2}$$

For $\boldsymbol{E}_{ext}\|\hat{z}$, this DM term promotes the canting of spins, favoring skyrmion formation, thus enhancing the formation of Néel-type skyrmion lattices over Bloch-type counterparts. Moreover, for a specific moiré length scale L_m, smaller values of q minimize the contribution from the polarization term, suggesting that the applied electric field can potentially alter the $k\pi$ value of the skyrmion lattice ground state.

For the sake of concreteness, we focus on the skyrmion lattice ground state, although all conclusions drawn here apply to higher order $k\pi$-skyrmion lattices. We focus on two distinct scenarios: subjecting the bilayer system to an external electric field in an adiabatic manner and a nonadiabatic manner. Adiabatically changing the external field strength involves incremental adjustment of the field in small steps while allowing for the spin configuration to relax adiabatically. In contrast, a nonadiabatic change involves applying a sudden change to the electric field, followed by a full relaxation of the spin configuration. The results of these calculations are shown in Figure 4. An adiabatic increase of the electric field preserves the

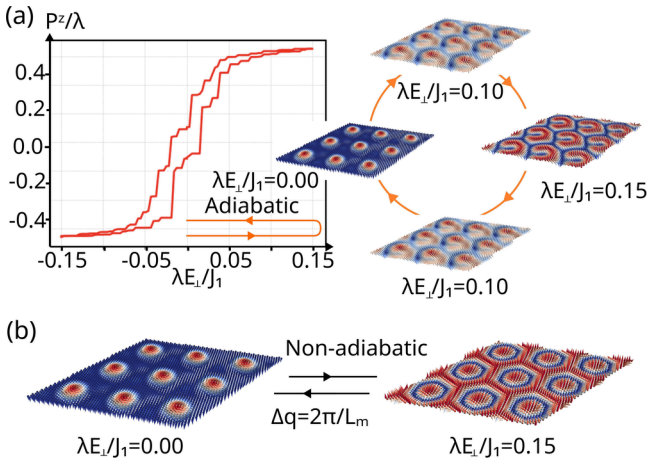

Figure 4. (a) Adiabatic evolution of the skyrmion lattice ground state of twisted NiI_2. The polarization along z for the top layer undergoes a hysteresis loop as the field magnitude $\lambda E_{ext}/J_1$ is changed along the loop $0 \rightarrow 0.15 \rightarrow -0.15 \rightarrow 0$ (b) Nonadiabatic evolution of the ground state, resulting in a transition from a skyrmion to a skyrmionium lattice. Only the top layer is shown for clarity, with the bottom one remaining antialigned with the top.

system's topological features, such as the nature of the skyrmion lattice, while merely deforming and shifting the location of the skyrmion center, originating a horseshoe skyrmion texture. Nevertheless, the hysteretic behavior of the system reflects the emergence of these topologically equivalent yet distinctly shaped spin ground state configurations. In this sense, varying L_m may allow for a more plastic deformation of the skyrmions, whereas smaller moiré unit cell sizes restrict the allowed skyrmionic solutions leading to sharper changes in behavior (see the Supporting Information for discussion on the interplay between the length-scales set by the interlayer interaction, field-induced DM interaction, and moiré length scale).

On the other hand, nonadiabatic changes lead to more dramatic effects, altering the k value in a $k\pi$-skyrmion. The skyrmion lattice can be transformed into a skyrmionium lattice through a nonadiabatic increase in the electric field. In this scenario, the external electric field effectively modifies the q of the underlying spin-spiral by $\Delta q = 2\pi/L_m$. Therefore, these results highlight the robustness and magnetoelectric tunability of the topological phases in twisted spin-spiral multiferroics.

We have demonstrated that twisted bilayer NiI_2 provides a highly tunable platform for engineering a whole family of topological magnetic phases. Our results establish that twist engineering allows stabilizing a variety of magnetic orders, including skyrmion lattices and nematic phases, thanks to the interplay between interlayer coupling and the moiré pattern.

https://doi.org/10.1021/acs.nanolett.4c04582
Nano Lett. 2024, 24, 15767−15773

The moiré-induced modulations stabilize nonuniform q-vector configurations, enabling complex magnetic textures and an out-of-plane ferroelectric polarization. The strong magnetoelectric coupling displayed by this twisted multiferroic allows for the manipulation of skyrmion lattice phases via an external electric field. These findings highlight the potential of twisted bilayer NiI_2 for exploring unconventional magnetism and ultimately enabling spintronics devices that exploit electric-field control of topological spin textures.

■ ASSOCIATED CONTENT

Supporting Information

The Supporting Information is available free of charge at https://pubs.acs.org/doi/10.1021/acs.nanolett.4c04582.

Details of numerical calculation of the reported spin ground states, density functional theory calculations of interlayer exchange modulation, effects of anisotropic symmetric exchange and relaxation, and details on the effects of external out-of-plane electric fields (PDF)

■ AUTHOR INFORMATION

Corresponding Authors

Tiago V. C. Antão − *Department of Applied Physics, Aalto University, 02150 Espoo, Finland;* orcid.org/0000-0003-3622-2513; Email: tiago.antao@aalto.fi

Jose L. Lado − *Department of Applied Physics, Aalto University, 02150 Espoo, Finland*; Email: jose.lado@aalto.fi

Adolfo O. Fumega − *Department of Applied Physics, Aalto University, 02150 Espoo, Finland;* orcid.org/0000-0002-3385-6409; Email: adolfo.oterofumega@aalto.fi

Complete contact information is available at: https://pubs.acs.org/10.1021/acs.nanolett.4c04582

Notes

The authors declare no competing financial interest.

■ ACKNOWLEDGMENTS

We acknowledge the computational resources provided by the Aalto Science-IT project and the financial support from the Academy of Finland Projects Nos. 331342, 358088, and 349696, the Jane and Aatos Erkko Foundation, and the Finnish Quantum Flagship. We thank M. Amini and P. Liljeroth for useful discussions.

■ REFERENCES

(1) Fert, A.; Cros, V.; Sampaio, J. Skyrmions on the track. *Nat. Nanotechnol.* **2013**, *8*, 152−156.

(2) Back, C.; Cros, V.; Ebert, H.; Everschor-Sitte, K.; Fert, A.; Garst, M.; Ma, T.; Mankovsky, S.; Monchesky, T. L.; Mostovoy, M.; et al. The 2020 skyrmionics roadmap. *J. Phys. D: Appl. Phys.* **2020**, *53*, 363001.

(3) Wang, K.; Bheemarasetty, V.; Duan, J.; Zhou, S.; Xiao, G. Fundamental physics and applications of skyrmions: A review. *J. Magn. Magn. Mater.* **2022**, *563*, 169905.

(4) Zhang, H.; Zhang, Y.; Hou, Z.; Qin, M.; Gao, X.; Liu, J. Magnetic skyrmions: materials, manipulation, detection, and applications in spintronic devices. *Materials Futures* **2023**, *2*, 032201.

(5) Kézsmárki, I.; Bordács, S.; Milde, P.; Neuber, E.; Eng, L. M.; White, J. S.; Rønnow, H. M.; Dewhurst, C. D.; Mochizuki, M.; Yanai, K.; Nakamura, H.; Ehlers, D.; Tsurkan, V.; Loidl, A. Néel-type skyrmion lattice with confined orientation in the polar magnetic semiconductor gav4s8. *Nat. Mater.* **2015**, *14*, 1116−1122.

(6) Powalla, L.; Birch, M. T.; Litzius, K.; Wintz, S.; Satheesh, S.; Weigand, M.; Goering, E.; Schütz, G.; Burghard, M. Skyrmion and skyrmionium formation in the two-dimensional magnet $cr_2ge_2te_6$. *Phys. Rev. B* **2023**, *108*, 214417.

(7) Zhang, Y.; Zhang, H.; Pang, J.; Ma, Y.; Zhang, M.; Xu, X.; Bellaiche, L. Generation of magnetic skyrmions in two-dimensional magnets via interfacial proximity. *Phys. Rev. B* **2023**, *107*, 024402.

(8) Yao, X.; Hu, D.; Dong, S. Modulation of skyrmionic magnetic textures in two-dimensional vdw materials and their heterostructures. *iScience* **2023**, *26*, 106311.

(9) Desautels, R. D.; DeBeer-Schmitt, L.; Montoya, S. A.; Borchers, J. A.; Je, S.-G.; Tang, N.; Im, M.-Y.; Fitzsimmons, M. R.; Fullerton, E. E.; Gilbert, D. A. Realization of ordered magnetic skyrmions in thin films at ambient conditions. *Phys. Rev. Mater.* **2019**, *3*, 104406.

(10) Li, X.; Liu, W. V.; Balents, L. Spirals and skyrmions in two dimensional oxide heterostructures. *Phys. Rev. Lett.* **2014**, *112*, 067202.

(11) Dzyaloshinsky, I. A thermodynamic theory of "weak" ferromagnetism of antiferromagnetics. *J. Phys. Chem. Solids* **1958**, *4*, 241−255.

(12) Moriya, T. New mechanism of anisotropic superexchange interaction. *Phys. Rev. Lett.* **1960**, *4*, 228−230.

(13) Mühlbauer, S.; Binz, B.; Jonietz, F.; Pfleiderer, C.; Rosch, A.; Neubauer, A.; Georgii, R.; Böni, P. Skyrmion lattice in a chiral magnet. *Science* **2009**, *323*, 915−919.

(14) Yuan, S.; Chen, Z.; Prokhorenko, S.; Nahas, Y.; Bellaiche, L.; Liu, C.; Xu, B.; Chen, L.; Das, S.; Martin, L. W. Hexagonal close-packed polar-skyrmion lattice in ultrathin ferroelectric $pbtio_3$ films. *Phys. Rev. Lett.* **2023**, *130*, 226801.

(15) Yu, X. Z.; Onose, Y.; Kanazawa, N.; Park, J. H.; Han, J. H.; Matsui, Y.; Nagaosa, N.; Tokura, Y. Real-space observation of a two-dimensional skyrmion crystal. *Nature* **2010**, *465*, 901−904.

(16) Okubo, T.; Chung, S.; Kawamura, H. Multiple-q states and the skyrmion lattice of the triangular-lattice heisenberg antiferromagnet under magnetic fields. *Phys. Rev. Lett.* **2012**, *108*, 017206.

(17) Shen, Y.; Zhang, Q.; Shi, P.; Du, L.; Yuan, X.; Zayats, A. V. Optical skyrmions and other topological quasiparticles of light. *Nat. Photonics* **2024**, *18*, 15−25.

(18) Stavrou, V. D.; Gergidis, L. N. Magnetic skyrmions generation and control in fept nanoparticles through shape and magnetocrystalline anisotropy variation: a finite elements method micromagnetic simulation study. *J. Phys. D: Appl. Phys.* **2021**, *54*, 285001.

(19) Seki, S.; Yu, X. Z.; Ishiwata, S.; Tokura, Y. Observation of skyrmions in a multiferroic material. *Science* **2012**, *336*, 198−201.

(20) Amoroso, D.; Barone, P.; Picozzi, S. Spontaneous skyrmionic lattice from anisotropic symmetric exchange in a ni-halide monolayer. *Nat. Commun.* **2020**, *11*, 5784.

(21) Das, J.; Akram, M.; Erten, O. Revival of antibiskyrmionic magnetic phases in bilayer nii_2. *Phys. Rev. B* **2024**, *109*, 104428.

(22) Geim, A. K.; Grigorieva, I. V. Van der waals heterostructures. *Nature* **2013**, *499*, 419−425.

(23) Burch, K. S.; Mandrus, D.; Park, J.-G. Magnetism in two-dimensional van der waals materials. *Nature* **2018**, *563*, 47−52.

(24) Gibertini, M.; Koperski, M.; Morpurgo, A. F.; Novoselov, K. S. Magnetic 2d materials and heterostructures. *Nat. Nanotechnol.* **2019**, *14*, 408−419.

(25) Blei, M.; Lado, J. L.; Song, Q.; Dey, D.; Erten, O.; Pardo, V.; Comin, R.; Tongay, S.; Botana, A. S. Synthesis, engineering, and theory of 2d van der waals magnets. *Applied Physics Reviews* **2021**, *8*, 021301.

(26) Cui, C.; Hu, W.-J.; Yan, X.; Addiego, C.; Gao, W.; Wang, Y.; Wang, Z.; Li, L.; Cheng, Y.; Li, P.; et al. Intercorrelated in-plane and out-of-plane ferroelectricity in ultrathin two-dimensional layered semiconductor in2se3. *Nano Lett.* **2018**, *18*, 1253−1258.

(27) Yuan, S.; Luo, X.; Chan, H. L.; Xiao, C.; Dai, Y.; Xie, M.; Hao, J. Room-temperature ferroelectricity in mote2 down to the atomic monolayer limit. *Nat. Commun.* **2019**, *10*, 1775.

(28) Ugeda, M. M.; Bradley, A. J.; Zhang, Y.; Onishi, S.; Chen, Y.; Ruan, W.; Ojeda-Aristizabal, C.; Ryu, H.; Edmonds, M. T.; Tsai, H.-Z.; et al. Characterization of collective ground states in single-layer nbse2. *Nat. Phys.* **2016**, *12*, 92−97.

(29) Fei, Z.; Huang, B.; Malinowski, P.; Wang, W.; Song, T.; Sanchez, J.; Yao, W.; Xiao, D.; Zhu, X.; May, A. F.; et al. Two-dimensional

itinerant ferromagnetism in atomically thin fe3gete2. *Nat. Mater.* **2018**, *17*, 778−782.
(30) Huang, B.; Clark, G.; Klein, D. R.; MacNeill, D.; Navarro-Moratalla, E.; Seyler, K. L.; Wilson, N.; McGuire, M. A.; Cobden, D. H.; Xiao, D.; et al. Electrical control of 2d magnetism in bilayer cri3. *Nat. Nanotechnol.* **2018**, *13*, 544−548.
(31) Lee, J.-U.; Lee, S.; Ryoo, J. H.; Kang, S.; Kim, T. Y.; Kim, P.; Park, C.-H.; Park, J.-G.; Cheong, H. Ising-type magnetic ordering in atomically thin feps3. *Nano Lett.* **2016**, *16*, 7433−7438.
(32) Gong, C.; Li, L.; Li, Z.; Ji, H.; Stern, A.; Xia, Y.; Cao, T.; Bao, W.; Wang, C.; Wang, Y.; et al. Discovery of intrinsic ferromagnetism in two-dimensional van der waals crystals. *Nature* **2017**, *546*, 265−269.
(33) Zhang, Z.; Shang, J.; Jiang, C.; Rasmita, A.; Gao, W.; Yu, T. Direct photoluminescence probing of ferromagnetism in monolayer two-dimensional crbr3. *Nano Lett.* **2019**, *19*, 3138−3142.
(34) Posey, V. A.; Turkel, S.; Rezaee, M.; Devarakonda, A.; Kundu, A. K.; Ong, C. S.; Thinel, M.; Chica, D. G.; Vitalone, R. A.; Jing, R.; et al. Two-dimensional heavy fermions in the van der waals metal cesii. *Nature* **2024**, *625*, 483−488.
(35) Song, T.; Sun, Q.-C.; Anderson, E.; Wang, C.; Qian, J.; Taniguchi, T.; Watanabe, K.; McGuire, M. A.; Stohr, R.; Xiao, D.; et al. Direct visualization of magnetic domains and moiré magnetism in twisted 2d magnets. *Science* **2021**, *374*, 1140−1144.
(36) Vano, V.; Amini, M.; Ganguli, S. C.; Chen, G.; Lado, J. L.; Kezilebieke, S.; Liljeroth, P. Artificial heavy fermions in a van der waals heterostructure. *Nature* **2021**, *599*, 582−586.
(37) Kezilebieke, S.; Huda, M. N.; Dreher, P.; Manninen, I.; Zhou, Y.; Sainio, J.; Mansell, R.; Ugeda, M. M.; van Dijken, S.; Komsa, H.-P.; Liljeroth, P. Electronic and magnetic characterization of epitaxial vse2 monolayers on superconducting nbse2. *Communications Physics* **2020**, *3*, 116.
(38) Andrei, E. Y.; Efetov, D. K.; Jarillo-Herrero, P.; MacDonald, A. H.; Mak, K. F.; Senthil, T.; Tutuc, E.; Yazdani, A.; Young, A. F. The marvels of moiré materials. *Nature Reviews Materials* **2021**, *6*, 201−206.
(39) Nuckolls, K. P.; Yazdani, A. A microscopic perspective on moiré materials. *Nature Reviews Materials* **2024**, *9*, 460−480.
(40) Fumega, A. O; Lado, J. L Moiré-driven multiferroic order in twisted crcl3, crbr3 and cri3 bilayers. *2D Materials* **2023**, *10*, 025026.
(41) Akram, M.; LaBollita, H.; Dey, D.; Kapeghian, J.; Erten, O.; Botana, A. S. Moiré skyrmions and chiral magnetic phases in twisted CrX_3 (x = i, br, and cl) bilayers. *Nano Lett.* **2021**, *21*, 6633−6639.
(42) Kim, K.-M.; Park, M. J. Controllable magnetic domains in twisted trilayer magnets. *Phys. Rev. B* **2023**, *108*, L100401.
(43) Shaban, P. S.; Lobanov, I. S.; Uzdin, V. M.; Iorsh, I. V. Skyrmion dynamics in moiré magnets. *Phys. Rev. B* **2023**, *108*, 174440.
(44) Xie, H.; Luo, X.; Ye, Z.; Sun, Z.; Ye, G.; Sung, S. H.; Ge, H.; Yan, S.; Fu, Y.; Tian, S.; et al. Evidence of non-collinear spin texture in magnetic moiré superlattices. *Nat. Phys.* **2023**, *19*, 1150−1155.
(45) Kim, K.-M.; Go, G.; Park, M. J.; Kim, S. K. Emergence of stable Meron quartets in twisted magnets. *Nano Lett.* **2024**, *24*, 74−81.
(46) Tong, Q.; Liu, F.; Xiao, J.; Yao, W. Skyrmions in the moiré of van der waals 2d magnets. *Nano Lett.* **2018**, *18*, 7194−7199.
(47) Xiao, F.; Chen, K.; Tong, Q. Magnetization textures in twisted bilayer Crx_3 (X = br,i). *Phys. Rev. Res.* **2021**, *3*, 013027.
(48) Haavisto, M.; Lado, J. L.; Otero Fumega, A. Topological multiferroic order in twisted transition metal dichalcogenide bilayers. *SciPost Physics* **2022**, *13*, 052.
(49) Abouelkomsan, A.; Bergholtz, E. J.; Chatterjee, S. Multiferroicity and topology in twisted transition metal dichalcogenides. *Phys. Rev. Lett.* **2024**, *133*, 026801.
(50) Akram, M.; Kapeghian, J.; Das, J.; Valenti, R.; Botana, A. S.; Erten, O. Theory of moiré magnetism in twisted bilayer α-rucl3. *Nano Lett.* **2024**, *24*, 890−896.
(51) Song, Q.; Occhialini, C. A.; Ergecen, E.; Ilyas, B.; Amoroso, D.; Barone, P.; Kapeghian, J.; Watanabe, K.; Taniguchi, T.; Botana, A. S.; et al. Evidence for a single-layer van der waals multiferroic. *Nature* **2022**, *602*, 601−605.
(52) Amini, M.; Fumega, A. O.; Gonzalez-Herrero, H.; Vano, V.; Kezilebieke, S.; Lado, J. L.; Liljeroth, P. Atomic-scale visualization of multiferroicity in monolayer nii2. *Adv. Mater.* **2024**, *36*, 2311342.
(53) Burch, K. S.; Mandrus, D.; Park, J.-G. Magnetism in two-dimensional van der waals materials. *Nature* **2018**, *563*, 47−52.
(54) Wang, Q. H.; Bedoya-Pinto, A.; Blei, M.; Dismukes, A. H.; Hamo, A.; Jenkins, S.; Koperski, M.; Liu, Y.; Sun, Q.-C.; Telford, E. J.; et al. The magnetic genome of two-dimensional van der waals materials. *ACS Nano* **2022**, *16*, 6960−7079.
(55) Liu, P.; Zhang, Y.; Li, K.; Li, Y.; Pu, Y. Recent advances in 2d van der waals magnets: Detection, modulation, and applications. *iScience* **2023**, *26*, 107584.
(56) Ramesh, R.; Spaldin, N. A. Multiferroics: progress and prospects in thin films. *Nat. Mater.* **2007**, *6*, 21−29.
(57) Fiebig, M.; Lottermoser, T.; Meier, D.; Trassin, M. The evolution of multiferroics. *Nature Reviews Materials* **2016**, *1*, 16046.
(58) Fumega, A. O.; Lado, J. L. Microscopic origin of multiferroic order in monolayer nii_2. *2D Materials* **2022**, *9*, 025010.
(59) Kurumaji, T.; Seki, S.; Ishiwata, S.; Murakawa, H.; Kaneko, Y.; Tokura, Y. Magnetoelectric responses induced by domain rearrangement and spin structural change in triangular-lattice helimagnets nii_2 and coi_2. *Phys. Rev. B* **2013**, *87*, 014429.
(60) Han, H.; Zheng, H.; Wang, Q.; Yan, Y. Enhanced magnetic anisotropy and curie temperature of the nii_2 monolayer by applying strain: a first-principles study. *Phys. Chem. Chem. Phys.* **2020**, *22*, 26917−26922.
(61) Kapeghian, J.; Amoroso, D.; Occhialini, C. A.; Martins, L. G. P.; Song, Q.; Smith, J. S.; Sanchez, J. J.; Kong, J.; Comin, R.; Barone, P.; et al. Effects of pressure on the electronic and magnetic properties of bulk nii_2. *Phys. Rev. B* **2024**, *109*, 014403.
(62) Liu, Q.; Su, W.; Gu, Y.; Zhang, X.; Xia, X.; Wang, L.; Xiao, K.; Cui, X.; Zou, Xi.; Xi, B; Mei, J.-W.; Dai, J.-F. Surprising pressure-induced magnetic transformations from helimagnetic order to antiferromagnetic state in nii2. *arXiv*, 2024, DOI: 10.48550/arXiv.2404.09569 (accessed 202-04-16).
(63) Liu, N.; Wang, C.; Yan, C.; Xu, C.; Hu, J.; Zhang, Y.; Ji, W. Competing multiferroic phases in monolayer and few-layer Nii_2. *Phys. Rev. B* **2024**, *109*, 195422.
(64) Lukovkina, A.; Lopez-Paz, S. A.; Besnard, C.; Guenee, L.; von Rohr, F. O.; Giannini, E. Controlling the magnetic properties of the van der waals multiferroic crystals co1−xnixi2. *Chem. Mater.* **2024**, *36*, 6237−6245.
(65) Riedl, K.; Amoroso, D.; Backes, S.; Razpopov, A.; Nguyen, T. P. T.; Yamauchi, K.; Barone, P.; Winter, S. M.; Picozzi, S.; Valenti, R. Microscopic origin of magnetism in monolayer 3*d* transition metal dihalides. *Phys. Rev. B* **2022**, *106*, 035156.
(66) Katsura, H.; Nagaosa, N.; Balatsky, A. V. Spin current and magnetoelectric effect in noncollinear magnets. *Phys. Rev. Lett.* **2005**, *95*, 057205.
(67) Mostovoy, M. Ferroelectricity in spiral magnets. *Phys. Rev. Lett.* **2006**, *96*, 067601.
(68) Jia, C.; Onoda, S.; Nagaosa, N.; Han, J. H. Bond electronic polarization induced by spin. *Phys. Rev. B* **2006**, *74*, 224444.
(69) Sødequist, J.; Olsen, T. Type II multiferroic order in two-dimensional transition metal halides from first principles spin-spiral calculations. *2D Materials* **2023**, *10*, 035016.
(70) Rybakov, A.; Fumega, A. O.; Esteras, D. L.; Lado, J. L.; Baldoví, J. J. Electrical control of magnons in multiferroic nii_2. *arXiv*, 2024, DOI: 10.48550/arXiv.2407.21645 (accessed 2024-08-02).
(71) Li, X.; Xu, C.; Liu, B.; Li, X.; Bellaiche, L.; Xiang, H. Realistic spin model for multiferroic nii_2. *Phys. Rev. Lett.* **2023**, *131*, 036701.
(72) Hayami, S.; Lin, S.-Z.; Batista, C. D. Bubble and skyrmion crystals in frustrated magnets with easy-axis anisotropy. *Phys. Rev. B* **2016**, *93*, 184413.
(73) Glittum, C.; Syljuasen, O. F. Arc-shaped structure factor in the J_1-J_2-J_3 classical heisenberg model on the triangular lattice. *Phys. Rev. B* **2021**, *104*, 184427.

https://doi.org/10.1021/acs.nanolett.4c04582
Nano Lett. 2024, 24, 15767−15773

(74) Kolesnikov, A. G.; Stebliy, M. E.; Samardak, A. S.; Ognev, A. V. Skyrmionium − high velocity without the skyrmion hall effect. *Sci. Rep.* **2018**, *8*, 16966.
(75) Wang, J.; Xia, J.; Zhang, X.; Zheng, X.; Li, G.; Chen, L.; Zhou, Y.; Wu, J.; Yin, H.; Chantrell, R.; Xu, Y. Magnetic skyrmionium diode with a magnetic anisotropy voltage gating. *Appl. Phys. Lett.* **2020**, *117*, 202401.
(76) Yang, S.; Zhao, Y.; Wu, K.; Chu, Z.; Xu, X.; Li, X.; Akerman, J.; Zhou, Y. Reversible conversion between skyrmions and skyrmioniums. *Nat. Commun.* **2023**, *14*, 3406.
(77) Yasuda, K.; Wang, X.; Watanabe, K.; Taniguchi, T.; Jarillo-Herrero, P. Stacking-engineered ferroelectricity in bilayer boron nitride. *Science* **2021**, *372*, 1458−1462.

https://doi.org/10.1021/acs.nanolett.4c04582
Nano Lett. 2024, 24, 15767−15773